JACS
JOURNAL OF THE AMERICAN CHEMICAL SOCIETY
Article
pubs.acs.org/JACS

Synthesis and Tunability of Highly Electron-Accepting, N-Benzylated "Phosphaviologens"

Monika Stolar, Javier Borau-Garcia, Mark Toonen, and Thomas Baumgartner*

Department of Chemistry and Centre for Advanced Solar Materials, University of Calgary, 2500 University Drive Northwest, Calgary, Alberta T2N 1N4, Canada

Supporting Information

ABSTRACT: We report a structure–property study on phosphoryl-bridged viologen analogues with a remarkably low reduction threshold. Utilizing different benzyl groups for N-quaternization, we were able to confirm the *p*-benzyl substituent effect on the electronic tunability of the system while maintaining the characteristic chromic response of viologens with two fully reversible one-electron reductions. Due to the considerably increased electron-acceptor properties of the phosphoryl-bridged bipyridine precursor, N-benzylation was found to be very challenging and required the development of new synthetic strategies toward the target viologen species. This study also introduces a new and convenient way for the anion exchange of viologen systems by utilizing methyl triflate. Finally, the practical utility of the new species was verified in simplified proof-of-concept electrochromic devices.

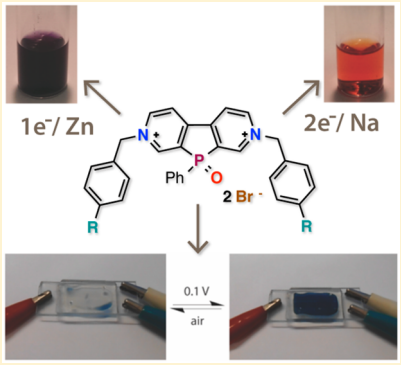

INTRODUCTION

The development of strongly electron-accepting π-conjugated materials has become a rapidly evolving state-of-the-art research area in recent years, due to their considerable potential for application in organic electronics and the fact that suitable acceptor materials are still quite rare.[1] One particularly intriguing class of materials in this context is bipyridinium species, which are formed upon N,N-diquaternization of 4,4′-bipyridine, also known as viologens (Chart 1).[2]

Chart 1

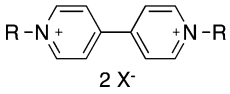

The extraordinary properties of the viologens have found widespread application in a host of most different fields that span from photochemistry,[3] electrochemistry,[4] and solar energy conversion[5] to molecular wires.[6] Viologens are frequently used as electrochemical label[7] or photochemical probe[8] or in studies on the electron-transport processes or oxidative damage in DNA.[9] Many of these applications are largely based on the viologens' ability to undergo reversible redox chemistry giving rise to three differently colored oxidation states (colorless, purple, and red/orange)[10,11] and the fact that the bipyridinium radical cations are among the most stable known organic radicals.[12,13] Moreover, the redox and electrochromic properties of viologens can usually be tuned via modification on the *N*-alkyl group (R), as well as the counteranion (X^-, Chart 1).[2] These features have also found practical utility in electrochromic applications such as self-dimming mirrors,[14] displays,[15] and, more recently, smart windows.[16]

While viologens themselves offer interesting electronic properties, the incorporation of additional heteroatoms can considerably enhance the electronic and optical properties of the materials. Phosphorus is of particular interest in this context due to its distinct pyramidal geometry, which leads to an energy-reduced lowest unoccupied molecular orbital (LUMO), especially when incorporated into cyclic, ring-fused organophosphorus structures, through negative hyperconjugation between the σ^* orbital of exocyclic substituents and the π-conjugated main scaffold.[17] We and others have been able to confirm enhanced electron-accepting capabilities for the resulting π systems, which make such species highly desirable for electronic applications.[18]

In 2011, we first reported the phosphorus-bridged viologen, *N*,*N*′-dimethyl-2,7-diazadibenzophosphole oxide **P-MV** (see Supporting Information for nomenclature). While we observed very similar redox behavior and electrochromic properties to those of methyl viologen, we were able to significantly lower the reduction threshold for both redox steps by 500 mV through the addition of the central five-membered phosphole oxide ring. The increased tendency for chemical reduction of the scaffold was confirmed via the significantly lowered LUMO level as a result from effective σ^*–π^* hyperconjugation.[19]

We have now focused our efforts toward further expanding the tunability of the reduction potentials of 2,7-diazadibenzophosphole oxide **1** (Scheme 1), through functionalization at the nitrogen atoms and modification of the counteranion. Herein

Received: December 30, 2014
Published: March 2, 2015

DOI: 10.1021/ja513258j
J. Am. Chem. Soc. 2015, 137, 3366–3371

Scheme 1. Synthesis of Benzylated 2,7-Diazadibenzophosphole Oxides[a]

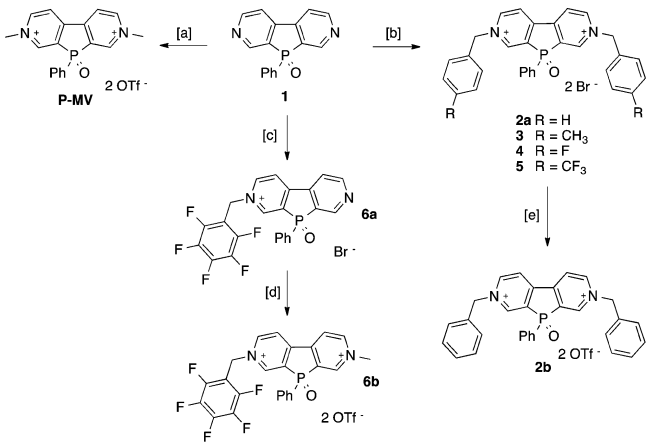

[a]Conditions: [a] MeOTf, 0 °C to RT, CH_2Cl_2;[19] [b] benzyl bromide, 60 °C, 72 h; [c] 2,3,4,5,6-pentafluorobenzyl bromide, 60 °C, 72 h; [d] MeOTf, 0 °C to RT, CH_2Cl_2; [e] MeOTf, 0 °C to RT, CH_2Cl_2 (carried out representatively with **2a**).

we report the results of using a series of substituted benzyl bromides for functionalization and electronic tuning. We provide alternative synthetic methods for efficient modification of the nitrogen centers via microwave conditions, along with the tunability of the electronic and optical properties of the new "phosphaviologens". Finally, we report our proof-of-concept efforts toward electrochromic devices.

RESULTS AND DISCUSSION

Development of a Suitable Synthetic Strategy. While solution-based N-benzylation of 4,4′-bipyridine has extensively been reported to be the method of choice,[20] it did not prove feasible for obtaining the targeted phosphorus-bridged dicationic salts at all. A series of solution-based synthetic attempts only resulted in mixtures of the mono- and dicationic salts, along with significant amounts of unreacted 2,7-diazadibenzophosphole oxide **1**, even after prolonged reaction times (days) and an excess of the respective benzyl bromide. This observation led us to determine the basicity of the nitrogen centers. Titration of 2,7-diazadibenzophosphole oxide with trifluoroacetic acid (TFAH) in CD_3CN (Supporting Information) revealed that the nitrogen centers in **1** have a significantly decreased basicity due to the electron-withdrawing effects of the phosphole oxide unit.[17,19] Consequently, we were unable to detect the fully N-protonated scaffold. The only detectable change was a gradual low-field shift of the pyridine ^{1}H resonances as well as a small high-field shifted ^{31}P NMR signal upon addition of TFAH that at least confirmed a weak association of the nitrogen centers with the acid (Supporting Information). To overcome this considerable synthetic challenge, neat reactions of **1** and the corresponding benzyl bromides were carried out at 60 °C over 72 h that resulted in the near quantitative formation of dicationic salts **2a−5** that could be isolated in moderate yields (55−65%) after simple filtration and precipitation from methanol into a diethyl ether/methanol/chloroform mixture (Scheme 1). The formation of the disubstituted symmetric products was confirmed by multinuclear NMR spectroscopy. The most revealing indication for the successful N-quaternization was the observed low-field shift of the α-pyridine protons from 9.0/8.9 to 9.9/9.5 ppm, respectively. In addition, the ^{31}P NMR spectra of **2a−5** showed a resonance at δ^{31}P = 30.3 ppm (irrespective of the 4-benzyl substituent) that is high-field shifted from that of **1** (cf.: 35.8 ppm).

To further accelerate the process, a neat reaction mixture was exposed to microwave conditions at 60 °C, which successfully resulted in the formation of the dicationic salt **2a** within 15 min, as opposed to the 72 h benchtop reaction.

While our new method proved feasible for several derivatives reported here, **1** could not be N,N-dialkylated with 2,3,4,5,6-pentafluorobenzyl bromide; the monobenzylated product **6a** was isolated instead. Even prolonged microwave conditions with 2,3,4,5,6-pentafluorobenzyl bromide only led to the formation of trace amounts of dibenzylated product, but we were never able to complete the reaction to a quantity that could be isolated and characterized. Monobenzylation of the isolated product **6a** was confirmed by the additional resonances in both the ^{1}H and the ^{13}C NMR spectra that supported an unsymmetrically substituted scaffold as well as the ^{31}P NMR resonance at δ^{31}P = 32.7 ppm. In order to obtain a dicationic salt with 2,3,4,5,6-pentafluorobenzyl bromide (which is evidently required for reversibly stable redox properties, see Supporting Information), we quaternized the second nitrogen center with excess methyl triflate in dichloromethane at room temperature over 2 h to give the asymmetric viologen analogue **6b** after a sequential anion exchange in situ (vide infra). Successful methylation of the remaining pyridine nitrogen center was clearly confirmed by additional resonances at δ = 4.52 and 48.6 ppm in the ^{1}H and ^{13}C NMR spectra, respectively, as well as a high-field-shifted ^{31}P resonance at

Table 1. Optical and Electronic Properties of Benzylated 2,7-Diazadibenzophosphole Oxides

compound	E_{red1} [mV][a]	E_{red2} [mV][a]	δE_{red} [mV][b]	λ_{max} [nm] (ε [L mol^{-1}cm^{-1}])[c]	λ_{max} [nm][d]	λ_{max} [nm][e]
P-MV	−602	−1032	430		406, 581, 634	408
2a	−536	−966	430	257 (6506), 294 (4936)	415, 584, 636	403
2b	−533	−967	434	257 (10 700), 298 (8270)	415 (5100)[f], 584 (3200)[f], 636 (3000)[f]	402 (7350)[f]
3	−554	−992	438	268 (11 906)	414, 583, 635	402
4	−537	−958	421	259 (10 978), 292 (8099)	415, 584, 636	402
5	−529	−940	411	259 (14 404), 293 (10 527)	415, 583, 636	398
6b	−538	−957	419	286 (16 369)	413, 581, 632	400
BnV	−839	−1226	387	262 (23 852)		

[a]CV in DMF solution with tetrabutylammonium hexafluorophosphate (0.05 M) as supporting electrolyte, referenced to Fc/Fc$^+$. [b]Difference between first and second reduction potentials. [c]UV−vis absorption in methanol. [d]Absorption maxima of radical species in CV solution. [e]Absorption maxima of neutral species in CV solution. [f]Determined in a spectroelectrochemical cell.

DOI: 10.1021/ja513258j
J. Am. Chem. Soc. 2015, 137, 3366−3371

δ^{31}P = 30.3 ppm, in line with the other diquaternized species **2a**–**5**.

To investigate the potential impact of the counteranion on the electrochemical behavior of the benzylated species, we also developed an anion exchange on **2a** using excess methyl triflate to efficiently obtain **2b** in dichloromethane at room temperature overnight. Notably, this new method is superior to the commonly applied anion exchange with silver triflate, as very little purification (i.e., simple filtration) is needed due to the volatility of the generated methyl bromide. Interestingly, the anion seems to impact the solid-state properties, evident in a charge transfer between anion and cation,[2] with **2a** being an orange and **2b** a white powder, respectively, but also the nature of the existing ion pairs in solution; the ^{31}P NMR spectrum of **2b** in CD_3OD showed a distinct high-field shift at δ^{31}P = 27.7 ppm. Further indication with regard to distinct cation–anion interactions in solution can be found in the absorption spectra of **2a** and **2b**, showing considerable differences in their extinction coefficients for the three main absorption peaks that appear at the same wavelengths otherwise (Table 1). Likely due to the considerable absorption properties of the bromide anion, compared to those of triflate, the extinction coefficients for **2a** have values that are roughly 60% of those observed for **2b**.

We were able to confirm the presence of several solid-state cation–anion interactions via **4**, for which we were able to obtain single crystals suitable for X-ray crystallography from a concentrated methanol solution. The anion–π interaction can clearly be seen in the space-filling diagram of the molecular structure of **4**, where one bromide is interacting closely with the phosphole ring π system at a distance of 3.2 Å while the other is participating in H–Br interactions with three neighboring hydrogen atoms at distances of 2.9–3.3 Å (Figure 1). In addition, the trans orientation of the two 4-fluorbenzyl substituents can be attributed to supramolecular packing effects. As confirmed via DFT calculations (see Supporting Information), the orientation of the benzyl substituents does not have any noticeable effect on the electronic properties of the main conjugated scaffold. Other pertinent metric parameters of the main scaffold (see Supporting Information) are largely similar to those of other related structurally characterized azadibenzophospholes,[17b] as well as **P-MV**,[19] and do not warrant any detailed discussion here.

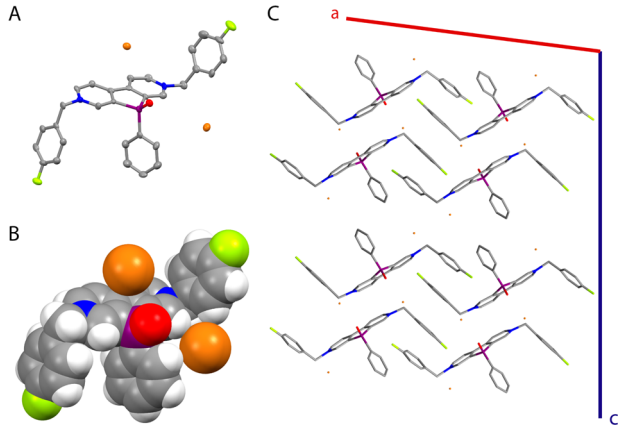

Figure 1. Solid-state structure of **4**, as obtained via single-crystal X-ray crystallography: (A) ellipsoids at 50% probability (H atoms omitted for clarity); (B) space-filling view; (C) molecular packing along the *b* axis of the unit cell.

Electrochemistry. The electrochemical properties of the new phosphaviologen species were investigated using cyclic voltammetry (CV), performed in DMF solutions; the results are summarized in Table 1. All dicationic species showed two reversible one-electron reductions (Figure 2A and Supporting Information) as previously observed with the dimethyl relative **P-MV**.[19] However, compared to the reduction features of **P-MV** under the same electrochemical conditions,[21] we were able to obtain a 66 mV lower reduction threshold for both reductions of **2a** and a record 73 and 92 mV lower reduction thresholds for the first and second reduction of **5**, respectively. In addition, the first reduction event of **2a** was 303 mV lower than the corresponding reduction of the parent analogue, 1,1′-bis(phenylmethyl)-4,4′-bipyridinium bromide (**BnV**), while the second reduction event occurred 260 mV lower under the same conditions. The latter clearly supports the strong electronic effect of the phosphoryl bridge on the viologen scaffold and the resulting lowered LUMO energy level. As also observed in related systems,[17b,19] the DFT-derived LUMO for **2a**,**b** largely comprises the delocalized π^* system of the conjugated backbone with contribution of the exocyclic P substituents. The LUMO clearly shows electron density contribution from both the exocyclic σ^* orbitals of the phenyl and the oxygen substituents, confirming the existence of σ^*–π^* hyperconjugation. In comparison, the LUMO of the twisted **BnV** only corresponds to its delocalized π^* system and is as such directly related to the LUMO of **2a**, pending the phosphoryl bridge (see Supporting Information for orbital visualizations). Notably, the LUMO level for **2a** (−4.05 eV) is lower than that

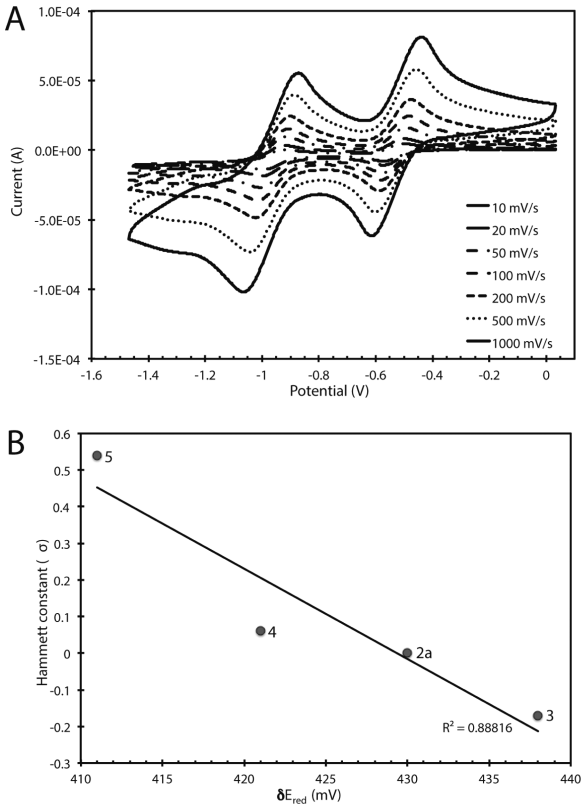

Figure 2. Cyclic voltammogram of **2a** (A) and Hammett plot vs δE_{red} (B).

DOI: 10.1021/ja513258j
J. Am. Chem. Soc. 2015, 137, 3366–3371

of **BnV** (cf. −3.73 eV) but also that of **P-MV** (cf. −3.77 eV),[19] suggesting that **2a** is more easily reduced, which is in line with the electrochemically obtained reduction potentials.

In order to further tune the electronic properties of the new species, we investigated the effects of the substituent at the 4 position on the benzyl ring, ranging from an electron-donating substituent (methyl) to two different electron-withdrawing substituents (fluoro, trifluoromethyl). As mentioned above, due to the lack of success in the synthesis of the diquaternized pentafluorobenzyl species, we instead utilized the asymmetric species **6b** to investigate the strength of one electron-withdrawing pentafluorobenzyl group. For the first reduction potential, we observed a difference of 25 mV between **3** (the most electron-donating substituent) and **5** (the most electron-withdrawing substituent). Remarkably, the substitution entailed a stronger effect on the second reduction event with a difference of 52 mV between **3** and **5**, demonstrating the effective tunability of the new system through small functional changes. In the case of the asymmetric pentafluoro species **6b**, we observed the first reduction at −538 mV, very similar to that of **2a** (cf. −536 mV). However, as seen with the other compounds in this series, the second reduction event is more strongly influenced by the quaternizing substituent, where we see a lowered potential of −957 mV for **6b**, compared to −966 mV for **2a**. A smaller reduction potential difference (δE_{red}) is consequently observed with increasing electron-withdrawing character in each species. Notably, δE_{red} can also be correlated reasonably well (R^2 = 0.89) with the Hammett constants of the 4-benzyl substituents, providing a trend that may guide further development of new phosphaviologenes with regard to adaptable redox potentials (Figure 2B).

As can be seen by the two reduction potentials for **2a** and **2b**, respectively, the counteranion does not have any notable effect on the redox properties of the main conjugated scaffold (ΔE = ±1−3 mV). The latter is not overly surprising, however, considering that the solution contains a large excess of PF_6^- from the electrolyte.

Spectroelectrochemistry. The photophysical properties of the new species were investigated via UV−vis spectroscopy in methanol for the dicationic salts (see Supporting Information) as well as in DMF for the mono- and direduced species in a spectroelectrochemical cell. While the absorption profiles of the dicationic salts are featureless and only show slight absorption in the UV region, confirming their optically transparent nature, the reduced species offered some impressive chromism. Using a spectroelectrochemical cell, we could isolate each of the three redox states of **2a**, providing a comparison of absorption profiles (Figure 3A). When no potential was applied to the cell, we observed the featureless absorption of the dication. However, upon addition of a potential preceding the first reduction threshold, the absorption features of the radical species with increased absorption throughout the visible spectrum could be seen. The production of the radical cation species of **2a** (**2a**′) was easily monitored over time, showing the saturation of color and increased absorption in the visible region of the optical spectrum (Figure 3C). Similarly, by applying a potential beyond the first reduction and preceding the threshold of the second reduction, we were able to observe the absorption profile of the neutral species **2a**″ in solution. The conversion of the radical species **2a**′ into the neutral species **2a**″ could be detected when monitoring the absorption over a period of time while constant potential was applied to the cell (Figure 3D). Interestingly, nearly identical absorption

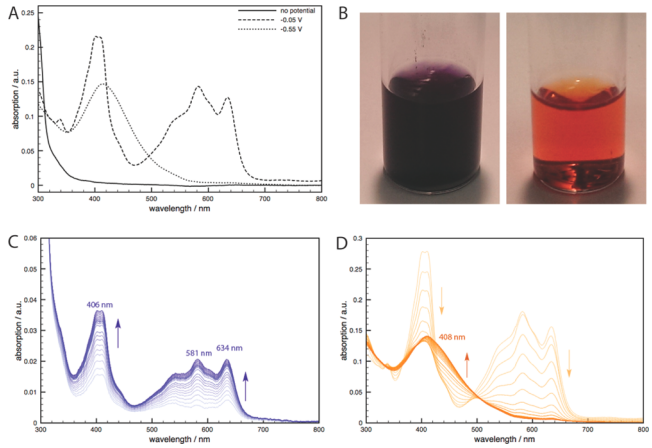

Figure 3. (A) UV−vis spectrum of isolated redox states of **2a**. (B) Chemical reduction of **2a**. (C) Isolated first reduction of **2a**. (D) Isolated second reduction of **2a**.

profiles were observed for the other species of this series (see Supporting Information), highlighting the fact that while we were able to tune the reduction potentials for these events by modification of the 4-benzyl position, the photophysical responses remain largely unaffected.

Notably, the reported compounds could also easily be chemically reduced to observe the pronounced color changes between the redox states in acetonitrile solution. Zinc dust was used to obtain the radical species **2a**′, evident in its deep blue-purple color, which was air stable for several minutes at room temperature and for several hours at −20 °C; sodium metal was used to obtain the bright orange neutral species **2a**″ (Figure 3B). Remarkably this species was still observed after the vial was left exposed to air overnight.

Radical Characterization. The radical nature of the singly reduced **2b**′ (as well as the radical cation of **P-MV**, see Supporting Information) was probed, for the first time, using electron paramagnetic resonance (EPR) spectroscopy in a flat cell at room temperature. To prepare the sample, **2b** was dissolved in dry and degassed acetonitrile; this solution was then added to a flask containing zinc dust under a nitrogen atmosphere. A small sample of the reduced species **2b**′ in solution was taken up by a syringe and filtered through an Acrodisc 0.2 μm PTFE membrane prior to injection into the flat cell. The resulting signal displayed a considerable amount of hyperfine coupling (Figure 4A), suggesting delocalization of the radical over a large portion of the molecular scaffold, as is also seen in parent viologens.[2] Both species, **P-MV** and **2b**′, had expected g-factor values of 2.034 and 2.031, respectively, supporting the organic nature of the radical. To gain more detailed insight into the nature of the radical, DFT calculations were performed at the B3LYP/6-31G(d) level of theory using the PCM solvation model and the spin density of the radical was modeled (Figure 4B).[22] The spin density calculations of the radical species indicate there is a strong correlation between the SOMO of the radical cation and the LUMO of the dicationic species, further supporting the fact that the observed reduction potentials are the result of the low energy level of the LUMO.

The DFT data also provided strong support for the radical being primarily delocalized and consequently stabilized over the entire π-conjugated scaffold of the molecule, in line with the observed EPR data. Using the calculated isotropic fermic

DOI: 10.1021/ja513258j
J. Am. Chem. Soc. 2015, 137, 3366−3371

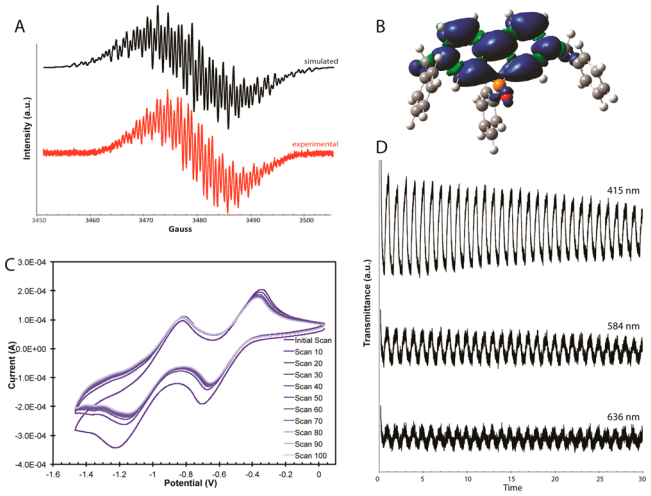

Figure 4. (A) EPR spectrum of **2b**′ (see Supporting Information for simulation parameters). (B) Spin density of the cationic portion of **2b**′ (B3LYP/6-31G(d) level of theory). (C) CV stability test of **2a**. (D) Absorption changes for electrochromic switching of **2a**.

contact couplings and the delocalization information from the spin density, the EPR spectrum of **2b**′ was simulated and is in good agreement with the experimentally observed EPR spectrum.

Stability Tests and Application in Electrochromic Devices. In order to test the viability of the new materials for potential electrochromic applications, we performed an electronic and photophysical stability test using CV and UV–vis spectroscopy, respectively. Since all of the compounds show similar electronic and photophysical properties, the tests were representatively performed using **2a**. Cyclic voltammetry was performed under the same conditions as described above, however, with a 100-scan cycle (Figure 4C). We observed minor changes in the CV from the initial scan to scan 40, likely due to diffusion effects present prior to reaching an equilibrated state,[23] but afterward stabilization upward to scan 100 is evident, indicating good electronic stability of the material, even after a large number of redox cycles. In addition, the minor deviation throughout the redox cycles does not seem to affect the reversibility of the redox events and is maintained throughout, making these materials indeed viable for long-term cycling in device applications. Moreover, the electrochromic switching of **2a** was tested in the same spectroelectrochemical cell. We probed each of the three major absorption peaks (415, 584, 636 nm) at separate intervals of 30 min, each with a 30 s delay in the potential switch between dicationic and radical species (Figure 4D). Reasonably good electrochromic switching was observed with the exception of the peak at 415 nm, where a slight decrease in the transmittance change occurred with an increased number of cycles. However, this decreased switching characteristic can be attributed to either diffusion of the radical species within the cell, which could leave residual radical species in solution prior to the cell switch, or different dynamic responses of the various species present in the bulk mixture. This was also observed at 584 and 636 nm but to a smaller extent, likely due to the decreased extinction coefficients at these wavelengths.

The proof-of-concept devices for this study, intended to verify electrochromic behavior, utilized fluorine-doped tin oxide (FTO)-coated glass as the electrodes and **2b** as active component, since the material is white/transparent in the solid state and thus the best candidate to give a colorless, fully transparent device redox state. Figure 5A shows the solution-based cell used to test the electrochromic behavior of **2b**. The two pieces of FTO glass were sealed together with a UV-cured gasket using a hardware gel. In order to further simplify the active components in the electrochromic device, we tested a cell without the use of a supporting electrolyte. To our satisfaction, a color change without the addition of a supporting electrolyte was observed, allowing us to develop electrochromic cells simply made from our materials dissolved in an appropriate solvent. However, while we were able to observe the electrochromic behavior, we were not able to demonstrate the reversibility within this particular device setting, as the strongly colored radical would simply build up on the opposite electrode but the entire cell would still appear to be the same color. To circumvent this occurrence, a second setup was constructed where the FTO was partially removed from each side of the glass slide before the cell was sealed with the UV-cured gasket. This second-generation device was then indeed able to display the expected reversibility of the electrochromism by alternating between positive and negative potentials (Figure 5B). Unfortunately we were not able to observe complete discoloration at any given time, as the cell thickness was too large (50 μm) and the colored radical species would diffuse through the solution at a rate faster than the potential switching. The movie in the Supporting Information demonstrates the switching behavior but is sped up 32 times to better visualize the redox switching. It should be mentioned in this context that state-of-the-art electrochromic devices require multilayer architectures and often a complex mixture of functional materials that fulfill the roles of electrodes, electrolyte, and active materials.[24] While our simplified proof-of-concept devices do not lend themselves for direct comparison in performance with the former, our studies nevertheless clearly establish the general dual applicability of **2b** as an electroactive component as well as an electrolyte in such a device setting.

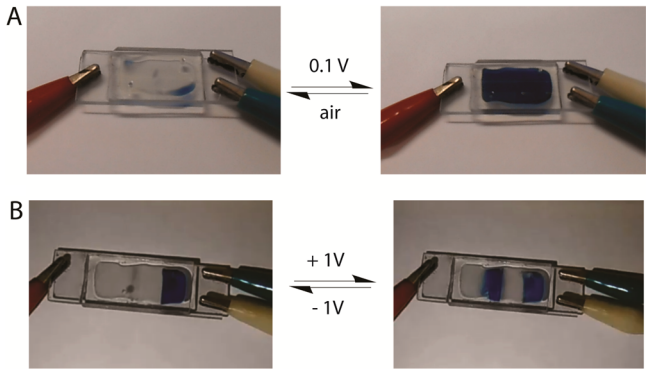

Figure 5. (A) Solution-based electrochromic device with **2b**. (B) Reversible solution-based device with **2b**.

CONCLUSIONS

We prepared a series of N,N-dibenzylated 2,7-diazadibenzophosphole oxides via newly developed synthetic protocols that allowed us to investigate the substituent effects on the electronic and photophysical properties of the materials. Furthermore, we developed a new method toward an efficient anion exchange for viologen species. Importantly, while we

DOI: 10.1021/ja513258j
J. Am. Chem. Soc. 2015, 137, 3366–3371

were able to noticeably lower the reduction potentials and to tune the electronic properties through introduction of either electron-donating or electron-withdrawing groups at the para position of the benzyl substituent, the various redox states preserve their colors (colorless, blue/purple, orange) in each of the species. This potentially opens the door for practical utility of the new materials in energy-efficient electrochromic applications. To this end, we designed simplified proof-of-concept electrochromic cells using the dibenzylated phosphaviologen **2b** as a representative example. However, while we have been able to achieve a simplistic device design with materials showing considerably lowered reduction threshold potential in the context of this initial study, an optimized material and/or device design is necessary prior to more sophisticated, large-scale applications. Corresponding studies are currently underway. In addition, to further extend the potential applications of our phosphaviologen materials beyond dimming devices, such as multicolored displays, investigations into obtaining differently colored redox states via modification of the main molecular scaffold are also currently being carried out.

■ ASSOCIATED CONTENT

Supporting Information

Full experimental details and characterization data of all new compounds; X-ray crystallographic data for **4**; comprehensive DFT data for all compounds and their reduced relatives (B3LYP/6-31G(d) level of theory); supporting movie showing the electrochromic switching in a device setting. This material is available free of charge via the Internet at http://pubs.acs.org.

■ AUTHOR INFORMATION

Corresponding Author

*thomas.baumgartner@ucalgary.ca

Author Contributions

The manuscript was written through contributions of all authors. All authors have given approval to the final version of the manuscript.

Notes

The authors declare no competing financial interest.

■ ACKNOWLEDGMENTS

Financial support by the Natural Sciences and Engineering Research Council of Canada (NSERC) and the Canada Foundation for Innovation is gratefully acknowledged. M.S. thanks NSERC and Alberta Innovates—Technology Futures for graduate scholarships. We thank Drs. T. C. Sutherland and C.-C. Ling for access to their instrumentation as well as D. Fox and W. White for support with the EPR spectroscopy.

■ REFERENCES

(1) (a) Stolar, M.; Baumgartner, T. *Phys. Chem. Chem. Phys.* **2013**, *15*, 9007−9024. (b) Eftaiha, A.; Sun, J.-P.; Hill, I. G.; Welch, G. C. *J. Mater. Chem. A* **2013**, *2*, 1201−1213.

(2) Monk, P. M. S. *The Viologens: Physicochemical Properties, Synthesis and Applications of the Salts of 4,4′-Bipyridine*; Wiley: Chichester, 1998.

(3) Ito, F.; Nagamura, T. *J. Photochem. Photobiol. C: Photochem. Rev.* **2007**, *8*, 174−190.

(4) Han, B.; Li, Z.; Li, C.; Pobelov, I.; Su, G.; Aguilar-Sanchez, R.; Wandlowski, T. *Top. Curr. Chem.* **2009**, *287*, 181−255.

(5) Fukuzumi, S. *Eur. J. Inorg. Chem.* **2008**, 1351−1362.

(6) Śliwa, W.; Bachowska, B.; Girek, T. *Curr. Org. Chem.* **2007**, *11*, 497−513.

(7) Takenaka, S.; Ihara, T.; Takagi, M. *J. Chem. Soc., Chem. Comm.* **1990**, 1485−1486.

(8) Fromherz, P.; Rieger, B. *J. Am. Chem. Soc.* **1986**, *108*, 5361−5362.

(9) (a) Bhattacharya, P. K.; Barton, J. K. *J. Am. Chem. Soc.* **2001**, *123*, 8649−8656. (b) Hariharan, M.; Joseph, J.; Ramaiah, D. *J. Phys. Chem. B* **2006**, *110*, 24678−24686. (c) Li, Y.; Yildiz, U. H.; Müllen, K.; Gröhn, F. *Biomacromolecules* **2009**, *10*, 530−540. (d) Holmlin, R. E.; Dandliker, P. J.; Barton, J. K. *Angew. Chem., Int. Ed.* **1997**, *36*, 2714−2730.

(10) Mortimer, R. J. *Electrochim. Acta* **1999**, *44*, 2971−2981.

(11) Li, M.; Wei, Y.; Zheng, J.; Zhu, D.; Xu, C. *Org. Electron.* **2014**, *15*, 428−434.

(12) Monk, P. M. S.; Mortimer, R. J.; Rosseinsky, D. R. *Electrochromism and Electrochromic Devices*; Cambridge University Press: Cambridge, 2007.

(13) Bamfield, P.; Hutchings, M. G. *Chromic Phenomena: Technological Applications of Colour Chemistry*; RSC Publishing: Cambridge, 2010.

(14) Bathe, S. R.; Patil, P. S. *J. Mater.* **2014**, 642069.

(15) Bonhote, P.; Gogniat, E.; Campus, F.; Walder, L.; Grätzel, M. *Displays* **1999**, *20*, 137−144.

(16) Granqvist, C. G.; Azens, A.; Hjelm, A.; Kullman, L.; Niklasson, G. A.; Rönnow, D.; Strømme Mattsson, M.; Veszelei, M.; Vaivars, G. *Sol. Energy* **1998**, *63*, 199−276.

(17) (a) Baumgartner, T. *Acc. Chem. Res.* **2014**, *47*, 1613−1622. (b) Durben, S.; Baumgartner, T. *Inorg. Chem.* **2011**, *50*, 6823−6836.

(18) (a) Ren, Y.; Baumgartner, T. *Dalton Trans.* **2012**, *41*, 7792−7800. (b) Stolar, M.; Baumgartner, T. *Chem.—Asian J.* **2014**, *9*, 1212−1225. (c) Takeda, Y.; Nishida, T.; Minakata, S. *Chem.—Eur. J.* **2014**, *20*, 10266−10270. (d) Worch, J. C.; Chirdon, D. N.; Maurer, A. B.; Qiu, Y.; Geib, S. J.; Bernhard, S.; Noonan, K. J. T. *J. Org. Chem.* **2013**, *78*, 7462−7469. (e) Washington, M. P.; Payton, J. L.; Simpson, M. C.; Protasiewicz, J. D. *Organometallics* **2011**, *30*, 1975−1983. (f) Tsuji, H.; Sato, K.; Sato, Y.; Nakamura, E. *J. Mater. Chem.* **2009**, *19*, 3364−3366. (g) Matano, Y.; Ohkubo, H.; Honsho, Y.; Saito, A.; Seki, S.; Imahori, H. *Org. Lett.* **2013**, *15*, 932−935. (h) Bruch, A.; Fukazawa, A.; Yamaguchi, E.; Yamaguchi, S.; Studer, A. *Angew. Chem., Int. Ed.* **2011**, *50*, 12094−12098.

(19) Durben, S.; Baumgartner, T. *Angew. Chem., Int. Ed.* **2011**, *50*, 7948−7952.

(20) (a) Sharrett, Z.; Gamsey, S.; Fat, J.; Cunningham-Bryant, D.; Wessling, R. A.; Singaram, B. *Tetrahedron Lett.* **2007**, *48*, 5125−5129. (b) Lamberto, M.; Rastede, E. E.; Decker, J.; Raymo, F. M. *Tetrahedron Lett.* **2010**, *51*, 5618−5620.

(21) Note: the redox properties of viologens are strongly dependent on the polarity of the solvent (ref 2). Since some of the new benzylated species are poorly soluble in acetonitrile, the redox properties of **P-MV** were reinvestigated in DMF solution to provide for a more suitable point of reference.

(22) Frisch, M. J.; et al. *Gaussian09*, Revision A.02; Gaussian, Inc.: Wallingford, CT, 2009 (see Supporting Information for full reference).

(23) Compton, R. G.; Banks, C. E. *Understanding Voltammetry*; Imperial College Press: London, 2011.

(24) (a) Sicard, L.; Navarathne, D.; Skalski, T.; Skene, W. G. *Adv. Funct. Mater.* **2013**, *23*, 3549−3559. (b) Knott, E. P.; Craig, M. R.; Liu, D. Y.; Babiarz, J. E.; Dyer, A. L.; Reynolds, J. R. *J. Mater. Chem.* **2012**, *22*, 4953−4962. (c) Moon, H. C.; Lodge, T. P.; Frisbie, C. D. *Chem. Mater.* **2015**, *27*, 1420−1425.

DOI: 10.1021/ja513258j
J. Am. Chem. Soc. 2015, 137, 3366−3371